# Mineralogical evolution of fayalite-bearing rapakivi granites from the Prins Christians Sund pluton, South Greenland

T. N. HARRISON[1], I. PARSONS[2] AND P. E. BROWN[1]*

[1]Department of Geology and Mineralogy, Aberdeen University, Aberdeen AB9 1AS, Scotland
[2]Grant Institute of Geology, University of Edinburgh, West Mains Road, Edinburgh EH9 3JW, Scotland

**Abstract**

The Prins Christians Sund rapakivi granite pluton in South Greenland is a member of the early Proterozoic 'Rapakivi Suite' and is emplaced into early Proterozoic Ketilidian migmatites. The pluton is composed predominantly of black or dark brown monzonites and quartz monzonites (collectively, rapakivi granites), although a localised white facies is developed adjacent to metasedimentary xenoliths. The back rapakivi granites are extremely fresh and have an anhydrous primary mafic mineralogy of olivine and orthopyroxene, with rare inverted pigeonite and clinopyroxene; minor amounts of biotite and amphibole occur in most fayalite-bearing rapakivi granites. Feldspars in these rocks are black and non-turbid. The white rapakivi granites have a wholly hydrous mafic silicate assemblage and turbid, white or cream-coloured feldspars. Electron microprobe analyses of the mafic silicates in the black rapakivi granites show that they are Fe-rich, comprising fayalite ($Fa_{93-96.5}$), orthopyroxene ($Fs_{77-81}$), ferro-pargasitic and ferro-edenitic hornblende (Fe/(Fe + Mg) = 0.72–0.93), and biotite (Fe/(Fe + Mg) = 0.77–0.88). Both biotite and amphibole crystallised subsolidus, and often adopt symplectic morphologies. Biotite has formed in response to a fayalite-consuming reaction at temperatures below 650–700°C and $f_{O_2}$ of $10^{-16.5}$ to $10^{-17.5}$ bars, and continued to grow under reducing conditions below the QFM buffer to temperatures below 450–500°C. Orthopyroxene formed in response to a low-pressure fayalite-consuming reaction in the melt. The correlation of black, pristine feldspar with anhydrous mafic silicates, and of turbid feldspar with hydrous phases suggests either that the feldspars reflect the anhydrous nature of the parent magma, or more likely that the mafic mineralogy of the white rapakivi granites is secondary.

KEYWORDS: Rapakivi granite, South Greenland, fayalite, subsolidus biotite.

## Introduction: geological setting

THE whole of Greenland south of latitude 61°45′N comprises the early Proterozoic Ketilidian mobile belt and associated intrusives (1.9–1.7 Ga). (Fig. 1*a*). At their extreme northwest boundary, the Ketilidian rocks comprise an extremely varied group of greenschist facies metasediments which lie unconformably upon Archaean gneisses, both deformation and metamorphic grade increasing to the southwest, The stratigraphy and structure of the belt has been extensively reviewed by Allaart (1976). Much of the central area of the mobile belt is occupied by the Julianehaab batholith, a large area of gneissose to massive granites and granodiorites, often characterised by spectacular net-veined diorite complexes (Windley, 1965; Allaart, 1967).

Ketilidian supracrustals to the south of this belt are largely semipelitic and psammitic migmatites, although acid metavolcanics are locally common. The metamorphic grade here lies generally in the upper amphibolite facies, although in the extreme southwest granulite facies hypersthene gneisses are associated with areas of extensive rapakivi granite magmatism (Bridgwater *et al.*, 1974). Cordierite, orthopyroxene, sillimanite, and garnet are common metamorphic index minerals, and *PT* estimates for the peak of regional metamorphism are 2–4 kbar and 700–800°C (Harrison *et al.*, 1988).

The culmination of the evolution of the Ketilidian occurred with the emplacement of large volumes of mafic and felsic magmas. The mafic

* Now at: Dept. of Geology, The University, St. Andrews, Fife KY16 9ST, Scotland.

*Mineralogical Magazine, March 1990, Vol. 54, pp. 57–66*

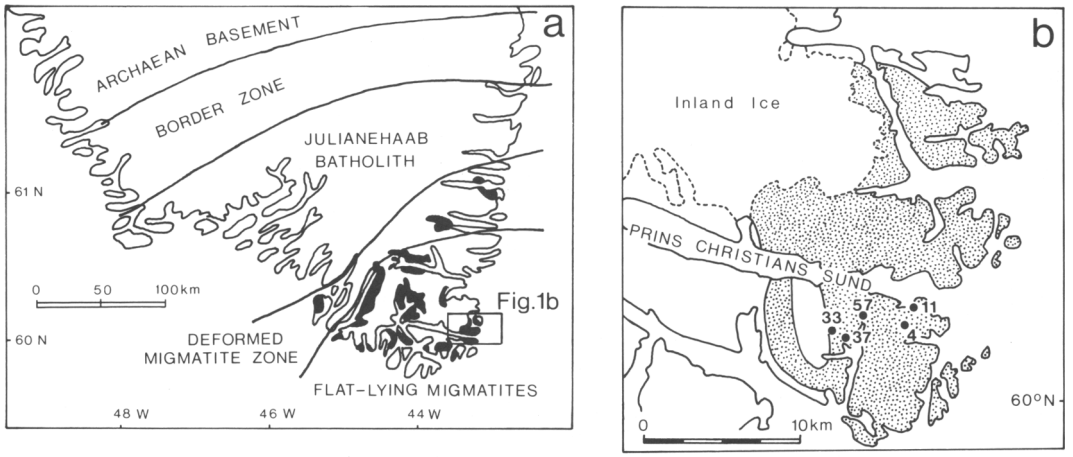


FIG. 1*a*. Major tectonic subdivisions of the Ketilidian mobile belt, South Greenland. Rapakivi granite plutons shown in black. Box shows the location of Fig. 1*b*. FIG. 1*b*. Geological sketch map of the Prins Christians Sund pluton showing the sample locations.

rocks form a very varied suite, ranging from rare picrites and layered olivine norites through to equigranular monzonorites, the latter dominating. The felsic rocks—the 'rapakivi granites'—are white or locally dark brown to black monzonites and quartz-monzonites (classification after Streckeisen, 1976), and are characterised by abundant K-feldspar ovoids (occasionally up to 15 cm across) which generally form 35 to 60% of the rock. Rapakivi texture (the mantling of K-feldspar by sodic plagioclase) is widely developed and is best seen in the white granites.

These rocks are locally intimately associated with the norites, and mafic material is seen injected into and chilled against rapakivi granite. Features such as lobate contacts and net-veining suggest the coexistence of two compositionally contrasting liquids (Bridgwater, 1963; Harrison *et al.*, in press); in general, however, the granites are later than the norites.

In terms of their bulk chemistry, the suite is a bimodal one and has tholeiitic affinities. Mafic compositions are characterised by Fe/(Fe + Mg) ratios >0.50, high $Al_2O_3$/CaO (>1.65), high Sr and Ba (often >1000ppm) and low Ni (<10ppm); their $SiO_2$ ranges from 50 to 55%. Felsic compositions have high Fe/(Fe + Mg) ratios (>0.65), lower Sr and Ba (300–500 ppm), and $SiO_2$ between 65 and 70%.

### The Prins Christians Sund pluton

The pluton lies at the eastern end of Prins Christians Sund (Fig. 1*b*) and relief is subdued (uncharacteristically for South Greenland), reaching 300–400 m. Exposure is excellent on the extensive coastline and also inland, as there is very little drift cover, although much of the eastern contact is covered by the inland ice-cap. The rapakivi granite is coarse-grained (grain-size over 5 cm) and is unusual amongst the South Greenland rapakivi plutons in being generally black or dark brown in hand specimen. A white facies is found only locally in areas where metasedimentary xenoliths are abundant, and can be seen to pass gradationally into the black facies. The black facies also contains xenoliths, although these are of microcline granite from the envelope. Aplites are rare, and pegmatites have not been recorded. A U–Pb zircon age of 1.733 Ga has been determined for the pluton (Gulson and Krogh, 1975).

The country rocks are predominantly composed of foliated microcline granite with thick concordant horizons of garnetiferous semipelitic migmatites. Garnet–cordierite–hypersthene gneisses (but no hornfelses) are developed at the contacts of the pluton, where local assimilation of metasediments and *lit-par-lit* veining are occasionally observed. Geobarometry and geothermometry (Table 1) on garnet–orthopyroxene–plagioclase–quartz assemblages in the aureole has yielded *PT* values of 2.6–4.5 kbar and 580–690°C. The low temperatures probably reflect a late hydration of the aureole as water was expelled from the pluton as it cooled, and late-stage biotite fringes are sometimes developed on garnet and orthopyroxene.

*TABLE 1. PT ESTIMATES FOR THE PRINS CHRISTIANS SUND PLUTON AUREOLE*

| | T(°C)[1] | P(kbars)[2] |
|---|---|---|
| Range | 580–690 | 2.6–4.5 |
| Mean | 620 (n=4) | 3.7 (n=4) |

*Method used*

1. Garnet-orthopyroxene (Harley, 1984).
2. Garnet-orthopyroxene-plagioclase-quartz; "Fe-reaction" (Perkins and Chipera, 1985).

## Petrography

All the members of the pluton are monzonites and quartz monzonites. Black or dark brown monzonites are characterised by a largely anhydrous primary mafic mineralogy, dominated by orthopryroxene with minor amounts of fayalitic olivine and Fe-rich amphibole. Biotite in these rocks commonly adopts a symplectic morphology. The white facies corresponds to quartz monzonite and has a wholly hydrous mafic silicate mineralogy, biotite often being dominant over amphibole. Rapakivi texture is developed throughout the pluton, but is more obvious in the white facies owing to the chalky-whiteness of the plagioclase rims. The white facies is often characterised by blue quartz. Both black and white facies are hereafter referred to as rapakivi granite. Five samples of fayalite-bearing (black) rapakivi granite have been selected for mineral analysis, although the assemblage is common throughout the pluton. Their locations are shown in Fig. 1*b*.

Most mineral analyses have been made using a Cambridge Instruments Geoscan electron microprobe with Link Systems energy-dispersive system and ZAF 4 corrections. However, three bulk analyses of alkali feldspar have been made using a Cameca Camebax wavelength dispersive instrument in Edinburgh University. Details of the analytical technique are given below.

## Olivine

Olivine is subhedral to anhedral, is largely unaltered, and is only found in the black facies. It is always enclosed by plagioclase and generally by K-feldspar, and often develops a crude symplectic intergrowth with groundmass quartz; it also occurs interstitial to quartz phenocrysts. Alteration is to brown 'iddingsite' and magnetite. Olivine is very Fe-rich with compositions between 93 and 96.5mol% Fa. (Table 2). Mn increases very slightly with increasing Fe content.

## Pyroxene

Most of the fayalite-bearing rapakivi granites contain orthopyroxene, which occurs in two habits. The commonest of these is as coarsely granular aggregates fringing olivine, although R1–11A also contains poikilitic crystals with clinopyroxene exsolution lamellae, suggestive of inverted pigeonite. No exsolution textures are seen in the granular orthopyroxene. Rare clinopyroxene (but no orthopyroxene) is present as a primary phase in R1–57, and R1–37 does not contain any pyroxene.

The chemistry of orthopyroxene is very similar in all analyses, the ratio Fe/(Fe + Mg) ranging from 0.793 ($Fs_{77}En_{20}Wo_2Rh_1$) to 0.838 ($Fs_{81}En_{16}Wo_{1.5}Rh_{1.5}$) (average 0.817; Table 2). However, similar compositional variation can also be observed in analyses from one sample (e.g. R1–33, Table 2). Unlike olivine, there is no correlation between Fe/(Fe + Mg) and Mn. Al contents are low in comparison with other Fe-rich orthopyroxenes (Deer *et al.*, 1978) and Al can generally be assigned in roughly equal amounts between tetrahedral and octahedral sites (Table 2). Ca contents are low except for R1–11A orthopyroxenes which contain up to 8 mol.% Wo (3.6 wt.% CaO). This feature may reflect the presence of submicroscopic clinopyroxene exsolution lamellae in the orthopyroxene. There is a good relationship between increasing Ca and Na in all orthopyroxenes. It has not been possible to analyse the clinopyroxene exsolution lamellae in the R1–11A orthopyroxenes. The clinopyroxene from R1–57 is ferroaugite of composition $Ca_{43}Mg_{14}Fe_{43}$ and Fe/(Fe + Mg) of 0.745.

## Amphibole

Amphibole is ubiquitous in the fayalite-bearing rapakivi granites and is bright green, displaying $a$ = yellowish green, $b$ = bluish green, $y$ = dark green pleochroism. It generally occurs as narrow interstitial poikilitic fringes around both olivine and orthopyroxene, and its textural relationships suggest a subsolidus origin. Crude symplectic intergrowths with quartz are often developed at the outer margins of the amphibole fringes. Amphibole in R1–11A occurs as large poikilitic plates which enclose the poikilitic orthopyroxene.

Amphibole compositions presented in Table 2 have been calculated using the FORTRAN programme FERRIC, lodged in the Department of Geology and Mineralogy, Aberdeen University. This is based on the IMA classification scheme of Leake (1978), with the assignation of $Fe^{3+}$ as

20% of total $Fe^{2+}$ using the method described by Brown *et al.*, (1982).

All the amphiboles are calcic, with $(Ca + Na)_B \geq 1.34$ and $(Na)_B < 0.67$, and within the IMA classification scheme they may be described predominantly as ferro-edenitic and ferro-pargasitic hornblende, although hastingsite and ferro-hornblende also occur. Like the accompanying mafic silicates the amphiboles have high Fe/(Fe + Mg) ratios, between 0.72 and 0.93. *A*-site occupancies do not show much variation, ranging between 0.439 and 0.713 Na + K atoms per formula unit. None of the other cations show any systematic variations with Fe/(Fe + Mg).

### Biotite

Biotite is found in all samples except R1–4. It occurs mostly as irregular fringes around amphibole, and is never seen in contact with olivine. Spectacular biotite–quartz symplectites are often developed at interfaces with both K-feldspar and plagioclase, and biotite may replace both plagioclase in myrmekite and perthitic microcline. Such textural relationships clearly demand a subsolidus origin. Biotite in R1–11A only occurs as poikilitic plates (up to 4 mm across) and does not develop any symplectic intergrowths.

Biotite is Fe-rich, the ratio Fe/(Fe + Mg) ranging from 0.770 to 0.880 (Table 2), and is comparatively rich in $Al^{vi}$, lying intermediate between phlogopite, annite, and siderophyllite. Despite the striking textural differences between biotite from R1–11A and other biotites, there is no observable compositional difference. $TiO_2$ contents are comparatively high and may reach up to 5.36 wt.%. F contents range from 0.32 to 0.60 wt.%.

### Feldspars

Alkali feldspar is subhedral to euhedral microcline with variable development of both cross-hatched twinning and microperthite. The twinning varies within single grains from readily visible to a fine tweed-like texture at the limit of optical resolution. The more coarsely twinned areas are sometimes obviously related to fractures and the development of turbidity, but this is not invariably the case as some coarsely twinned areas are free from turbidity. Feldspar in the black rapakivi granites is largely, but not wholly, devoid of turbidity. Work currently in progress (F. D. L. Walker and I. Parsons, Edinburgh University) shows that the turbidity is caused by micropores, mostly on the sub-micrometre scale. It is considered that the absence of such pores imparts the distinctive colour to the black rapakivi granites.

The microline contains various developments or microperthite. In the clear crystals the albite is in the form of thin or blunt lenses on a variety of scales from approximately 1 μm to 0.05 mm; some areas of microcline appear to be free of perthite. It is extremely laborious to obtain meaningful bulk compositions of such grains, but a set of three microprobe traverses has been made across large black microclines in R1–11A, using a step interval typically of 25 μm and analysing with a 1 μm beam rastered over an area of 10 $\mu m^2$. This gave the average compositions shown in Table 2. The low bulk albite and anorthite contents are consistent with equilibration of the bulk crystal at a low temperature (less than *c.* 700°C; Furhman and Lindsley, 1988).

The microcline composition ranges from about $Or_{75}Ab_{24}An_1$ to $Or_{88}Ab_{11.5}An_{0.5}$ The albite-rich lamellae were too thin to analyse with the microprobe, but extrapolation of the mixing line obtained on the traverses would imply albite–oligoclase in the range $An_8$-$An_{27}$. The most Ca-rich point analysed on the mixing line was $Or_{42}Ab_{43}An_{15}$.

Perthite in the turbid feldspars is less regular and more coarsely developed. The connection between turbidity in feldspars and perthite coarsening was illustrated by Parsons (1978), who discussed the evidence that fluid–rock interactions were responsible. Recently, Worden *et al.* (1989) have provided microtextural detail and demonstrated the pervasive nature of these interactions. In this context, it is interesting to note that the alkali feldspars from the black rapakivi granite have markedly higher BaO (0.8–1.35 wt.%) than those from the white granite (less than 0.5 wt.%).

The microcline crystals also contain larger (typically 0.1 mm), more angular crystals of albite and pericline-twinned plagioclase, frequently similarly orientated in parts of the microlines, but not consistently throughout the crystal. This suggests replacement of earlier plagioclase, rather than a perthitic relationship. The microclines often appear to be broken up into slightly disorientated domains as though annealing followed earlier deformation. The rather striking variability in coarseness of the twin texture, and its variable relationship with the occasional turbidity, is also consistent with a multiphase history for these crystals. The youngest event would be the development of the turbidity and associated coarsening of exsolution textures and twins. Parsons and Brown (1984) have shown that in syenitic rocks these interactions occur at temperatures less than *c.* 450°C, a view supported by the recent work of Worden *et al.* (1989).

Plagioclase is subhedral to euhedral and is the

*TABLE 2. REPRESENTATIVE ELECTRON MICROPROBE ANALYSES OF OLIVINE, PYROXENE, BIOTITE, FELDSPAR, ILMENITE, AND AMPHIBOLE*
*ALL SAMPLES ARE PREFIXED WITH R1; n.a. - NOT ANALYSED*

| | Olivine | | | | | Orthopyroxene | | | Clino-pyroxene | Biotite | | | |
|---|---|---|---|---|---|---|---|---|---|---|---|---|---|
| SAMPLE | 4 | 11A | 33 | 37 | 57 | 4 | 11A | 33 | 57 | 11A | 33 | 37 | 57 |
| $SiO_2$ | 30.49 | 30.58 | 30.21 | 30.11 | 30.40 | 47.47 | 47.55 | 47.32 | 49.37 | 35.49 | 34.62 | 33.73 | 34.00 |
| $TiO_2$ | 0.00 | 0.06 | 0.00 | 0.00 | 0.00 | 0.04 | 0.22 | 0.11 | 0.26 | 4.66 | 5.36 | 3.82 | 4.15 |
| $Al_2O_3$ | 0.11 | 0.00 | 0.01 | 0.05 | 0.00 | 0.26 | 0.24 | 0.36 | 0.70 | 13.69 | 13.69 | 13.88 | 14.11 |
| FeO | 66.29 | 66.44 | 65.67 | 66.22 | 66.41 | 44.63 | 41.75 | 44.20 | 24.03 | 29.45 | 28.20 | 32.79 | 30.79 |
| MnO | 0.94 | 0.96 | 1.40 | 1.95 | 1.61 | 0.83 | 0.56 | 0.82 | 0.57 | 0.03 | 0.11 | 0.09 | 0.10 |
| MgO | 2.36 | 2.08 | 2.14 | 0.95 | 1.51 | 5.37 | 5.26 | 5.53 | 4.59 | 4.87 | 4.00 | 2.54 | 3.62 |
| CaO | 0.02 | 0.00 | 0.09 | 0.01 | 0.08 | 0.52 | 3.60 | 0.55 | 20.19 | 0.04 | 0.04 | 0.01 | 0.06 |
| $Na_2O$ | n.a. | n.a. | n.a. | n.a. | n.a. | 0.34 | 0.19 | 0.02 | 0.17 | 0.24 | 0.27 | 0.29 | 0.00 |
| $K_2O$ | n.a. | n.a. | n.a. | n.a. | n.a. | n.a. | n.a. | n.a. | n.a. | 9.20 | 9.38 | 9.16 | 9.11 |
| F | | | | | | | | | | 0.60 | 0.32 | 0.47 | 0.55 |
| Cl | | | | | | | | | | 0.03 | 0.08 | 0.12 | 0.06 |
| Total | 100.21 | 100.12 | 99.52 | 99.29 | 100.01 | 99.46 | 99.37 | 99.11 | 99.72 | 98.30 | 96.07 | 96.90 | 96.49 |
| *Structural formulae calculated for number of anions:* | | | | | | | | | | | | | |
| | 4 | 4 | 4 | 4 | 4 | 6 | 6 | 6 | 6 | 24(OH, F, Cl) | | 24 | 24 |
| Si | 1.004 | 1.011 | 1.005 | 1.011 | 1.009 | 2.000 | 1.993 | 1.997 | 1.977 | 5.567 | 5.490 | 5.490 | 5.488 |
| $Al^{iv}$ | | | | | | 0.000 | 0.007 | 0.003 | 0.023 | 2.433 | 2.510 | 2.150 | 2.512 |
| $Al^{vi}$ | 0.004 | 0.000 | 0.000 | 0.002 | 0.000 | 0.013 | 0.005 | 0.015 | 0.010 | 0.099 | 0.049 | 0.153 | 0.173 |
| Ti | 0.000 | 0.001 | 0.000 | 0.000 | 0.000 | 0.001 | 0.007 | 0.004 | 0.008 | 0.550 | 0.639 | 0.468 | 0.504 |
| Fe | 1.826 | 1.836 | 1.828 | 1.860 | 1.843 | 1.573 | 1.464 | 1.568 | 0.808 | 3.863 | 3.740 | 4.563 | 4.156 |
| Mn | 0.026 | 0.027 | 0.039 | 0.056 | 0.045 | 0.030 | 0.020 | 0.029 | 0.020 | 0.004 | 0.015 | 0.012 | 0.014 |
| Mg | 0.116 | 0.103 | 0.106 | 0.047 | 0.075 | 0.337 | 0.328 | 0.348 | 0.275 | 1.138 | 1.151 | 0.616 | 0.871 |
| Ca | 0.001 | 0.000 | 0.003 | 0.000 | 0.003 | 0.024 | 0.162 | 0.025 | 0.869 | 0.007 | 0.007 | 0.002 | 0.010 |
| Na | | | | | | 0.028 | 0.016 | 0.001 | 0.013 | 0.073 | 0.083 | 0.092 | 0.000 |
| K | | | | | | | | | | 1.841 | 1.898 | 1.902 | 1.876 |
| F | | | | | | | | | | 0.307 | 0.161 | 0.241 | 0.278 |
| Cl | | | | | | | | | | 0.008 | 0.022 | 0.033 | 0.016 |
| Total | 2.977 | 2.978 | 2.981 | 2.976 | 2.975 | 4.006 | 4.001 | 3.989 | 4.006 | 15.890 | 15.762 | 15.981 | 15.897 |
| Fe/(Fe+Mg) | 0.940 | 0.946 | 0.945 | 0.975 | 0.960 | 0.823 | 0.817 | 0.818 | 0.746 | 0.772 | 0.798 | 0.879 | 0.827 |
| $X_{Mg}$ | | | | | | | | | | 0.858 | 0.910 | 0.870 | 0.853 |

| | K-feldspar | | | | | Plagioclase | | Ilmenite | | Amphibole | | | | |
|---|---|---|---|---|---|---|---|---|---|---|---|---|---|---|
| SAMPLE | 4 | 11A n=18 | 11A n=19 | 11A n=21 | 57 | 4 | 57 | 11A | 37 | 4 | 11A | 33 | 37 | 57 |
| $SiO_2$ | 65.09 | 64.54 | 64.33 | 63.98 | 64.54 | 60.13 | 58.48 | 0.38 | 0.27 | 40.64 | 40.09 | 40.75 | 39.95 | 39.96 |
| $TiO_2$ | n.a. | n.a. | n.a. | n.a. | n.a. | n.a. | n.a. | 50.67 | 50.71 | 1.49 | 1.09 | 2.06 | 0.63 | 0.82 |
| $Al_2O_3$ | 18.85 | 19.18 | 19.24 | 19.51 | 18.59 | 25.17 | 25.71 | 0.06 | 0.01 | 9.58 | 10.96 | 10.43 | 10.93 | 11.52 |
| FeO | 0.00 | 0.03 | 0.03 | 0.03 | 0.00 | 0.09 | 0.11 | 47.58 | 47.22 | 26.92 | 27.32 | 27.45 | 30.07 | 28.32 |
| MnO | n.a. | n.a. | n.a. | n.a. | n.a. | n.a. | n.a. | 0.51 | 1.06 | 0.36 | 0.25 | 0.16 | 0.32 | 0.42 |
| MgO | n.a. | 0.01 | 0.01 | 0.01 | n.a. | n.a. | n.a. | 0.20 | 0.09 | 4.46 | 3.95 | 3.45 | 2.20 | 2.69 |
| CaO | 0.10 | 0.16 | 0.28 | 0.43 | 0.04 | 6.94 | 8.18 | 0.02 | 0.01 | 10.40 | 10.74 | 10.99 | 10.64 | 10.72 |
| $Na_2O$ | 1.94 | 2.12 | 2.32 | 3.05 | 1.39 | 7.38 | 6.61 | n.a. | n.a. | 1.68 | 1.58 | 1.70 | 1.59 | 1.50 |
| $K_2O$ | 13.93 | 13.88 | 13.44 | 12.11 | 14.81 | 0.23 | 0.32 | n.a. | n.a. | 1.42 | 1.55 | 1.43 | 1.35 | 1.50 |
| Total | 99.91 | 99.93 | 99.65 | 99.19 | 99.37 | 99.94 | 99.41 | 99.42 | 99.37 | 96.95 | 97.53 | 98.42 | 97.68 | 97.45 |
| *Structural formulae calculated for number of anions:* | | | | | | | | | | | | | | |
| | 32 | 32 | 32 | 32 | 32 | 32 | 32 | 6 | 6 | 23 | 23 | 23 | 23 | 23 |
| Si | 11.930 | 11.864 | 11.844 | 11.788 | 11.932 | 10.715 | 10.520 | 0.019 | 0.014 | 6.509 | 6.396 | 6.436 | 6.441 | 6.405 |
| Al | 4.073 | 4.158 | 4.177 | 4.239 | 4.050 | 5.287 | 5.451 | 0.004 | 0.001 | 1.491 | 1.604 | 1.564 | 1.559 | 1.595 |
| Ti | | | | | | | | 1.944 | 1.950 | 0.317 | 0.456 | 0.559 | 0.518 | 0.583 |
| Fe | 0.000 | 0.002 | 0.002 | 0.002 | 0.000 | 0.013 | 0.016 | 2.030 | 2.019 | 0.432 | 0.409 | 0.166 | 0.439 | 0.357 |
| Mn | | | | | | | | 0.022 | 0.046 | 2.957 | 3.032 | 3.376 | 3.395 | 3.262 |
| Mg | | | | | | | | 0.015 | 0.007 | 0.180 | 0.131 | 0.244 | 0.076 | 0.099 |
| Ca | 0.019 | 0.032 | 0.055 | 0.099 | 0.008 | 1.324 | 1.577 | 0.001 | 0.001 | 1.065 | 0.939 | 0.813 | 0.528 | 0.642 |
| Na | 0.690 | 0.755 | 0.828 | 1.089 | 0.497 | 2.550 | 2.307 | | | 0.049 | 0.033 | 0.022 | 0.044 | 0.057 |
| K | 3.257 | 3.255 | 3.156 | 2.846 | 3.493 | 0.052 | 0.074 | | | 1.785 | 1.837 | 1.861 | 1.838 | 1.842 |
| | | | | | | | | | | 0.215 | 0.163 | 0.139 | 0.162 | 0.158 |
| | | | | | | | | | | 0.307 | 0.327 | 0.381 | 0.334 | 0.309 |
| | | | | | | | | | | 0.290 | 0.315 | 0.288 | 0.277 | 0.306 |
| Total | 19.971 | 20.066 | 20.062 | 20.063 | 19.981 | 19.942 | 19.945 | 4.035 | 4.036 | 15.597 | 15.642 | 15.669 | 15.611 | 15.615 |
| | | | | | | | | | | Fe/(Fe+Mg) | 0.761 | 0.786 | 0.813 | 0.879 | 0.849 |
| | | | | | | | | | | Name | FEH | FPH | FPH | FPH | FPH |

FEH Ferro-edenitic hornblende
FPH Ferro-pargasitic hornblende
Names after Leake (1978)

*TABLE 3. DATA USED IN EQUATION (3) TO DERIVE BIOTITE STABILITY CURVES SHOWN IN FIGS. 2 AND 3.*

| | $X_{Fe}^{Bio}$ | $X_{OH}^{Bio}$ | $a_{San}^{Afsp}$ | $a_{Fa}^{Ol}$ |
|---|---|---|---|---|
| R1-11A | 0.685 | 0.858 | 0.80 | 0.950 |
| R1-33 | 0.686 | 0.910 | 0.80 | 0.945 |
| R1-37 | 0.781 | 0.870 | 0.80 | 0.980 |
| R1-57 | 0.727 | 0.853 | 0.80 | 0.955 |

first of the major phases to have crystallised. It often displays weak zoning, and patches of blebby antiperthite are widely developed. Myrmekite is ubiquitous. Plagioclase is often strongly deformed even though other phases do not appear so. Compositions range between $An_{33}$ and $An_{43}$ (Table 2) and although zoning is optically detectable, there is no significant compositional difference between rims and cores. Antiperthite lamellae have compositions around $Or_{96}Ab_4$.

### Accessory minerals

Accessory minerals include ilmenite, apatite, large lilac-coloured zircons, and allanite. No primary magnetite has been observed, although secondary magnetite is seen as an alteration product of olivine. Ilmenite occurs as small, discrete grains, commonly associated with mafic silicates, and is free from exsolution lamellae. The composition of ilmenite is very similar in all fayalite-bearing assemblages (Table 2), and approaches that of end-member ilmenite. Mn and Si are present in all analyses, the former up to 1.18 wt.% MnO.

### Interpretation of mineral chemistry

*Mineral tie-lines*. Tie-line configurations of the mafic silicates show that Fe/(Fe + Mg)Ol >Fe/(Fe + Mg) Opx> Fe/(Fe + Mg) Amp, Bio. In R1–57 all mafic silicates have Fe/(Fe + Mg) greater than that of clinopyroxene. Similar relationships have been noted from the data of Smith (1974), Oyawoye and Makanjuola (1972) and Frisch and Bridgwater (1976) from other Fe-rich felsic intrusives and may reflect changing Fe–Mg partitioning in both the evolving magma and in the subsolidus.

*Equilibria involving biotite*. The use of Fe–Ti oxide pairs to estimate $T$–$f_{O_2}$ conditions is not applicable to any of the samples as no primary magnetite is present. However, the presence of the assemblages Ol + Qtz + Bio + K-fspar means that $T$–$f_{O_2}$ estimates can be made using the reactions:

$$\underset{\text{sanidine}}{KalSi_3O_8} + \underset{\text{magnetite}}{Fe_3O_4} + H_2O = \underset{\text{biotite}}{KFe_3AlSi_3O_{10}(OH)_2} + 1/2O_2, \quad (1)$$

$$\underset{\text{biotite}}{KFe_3Alsi_3O_{10}(OH)_2} + 3/2\underset{\text{quartz}}{SiO_2} = \underset{\text{sanidine}}{KAlSi_3O_8} + 3/2\underset{\text{fayalite}}{Fe_2SiO_4} + H_2O. \quad (2)$$

The absence of magnetite in the fayalite-bearing rapakivi granites suggests that either reaction (1) has proceeded to completion, or that $f_{O_2}$ was intrinsically low (i.e. below QFM) throughout the evolution of the mineral assemblages. The presence of fayalite as an early phase lends some credence to this latter argument.

Reaction (1) can be represented by

$$\log f_{H_2O} = \frac{7409}{T} + 4.25 + 3\log X_{Fe}^{Bio} + 2\log X_{OH}^{Bio} - 1/2\log f_{O_2} - \log a_{San}^{Afsp} - \log a_{Mt}^{Sp} \quad (3)$$

(Czamanske and Wones, 1973), and calculated biotite stabilities for this reaction are shown in Fig. 2. The curves are calculated on the assumption that biotite would have been in equilibrium with magnetite having $a_{Mt}^{Sp}$ (equivalent to $X_{Mt}^{Sp}$) of 0.9; bearing in mind the near end-member composition of the ilmenite, this assumption seems reasonable. As such, they should only be regarded as limiting curves. $a_{San}^{Afsp}$ is taken as 0.8, and other values for $X_{Fe}^{Bio}$ and $X_{OH}^{Bio}$ are given in Table 3.

Also shown on Fig. 2 are the upper stabilities of the assemblage biotite + quartz (Eugster and Wones, 1962) for the range of biotite Fe/(Fe + Mg) in the fayalite-bearing rapakivi granites. The intersection of these curves with the biotite stability curves defined by reaction (1) indicates that biotite crystallisation commenced in the range 700–650°C at an $f_{O_2}$ of approximately $10^{-16.5}$ to $10^{-17.5}$ bars. The continued persistence of fayalite on the liquidus until a late stage indicates a reducing trend, and this trend was maintained throughout the subsolidus evolution of the rapakivi granites.

The stability curve for synthetic ferropargasite buffered by QFM is also shown in this figure (after Gilbert, 1966) as this amphibole approaches the composition of many of those seen in the fayalite-bearing rapakivi granites (Table 2). Gilbert (1966) has shown that the assemblage ferropargasite

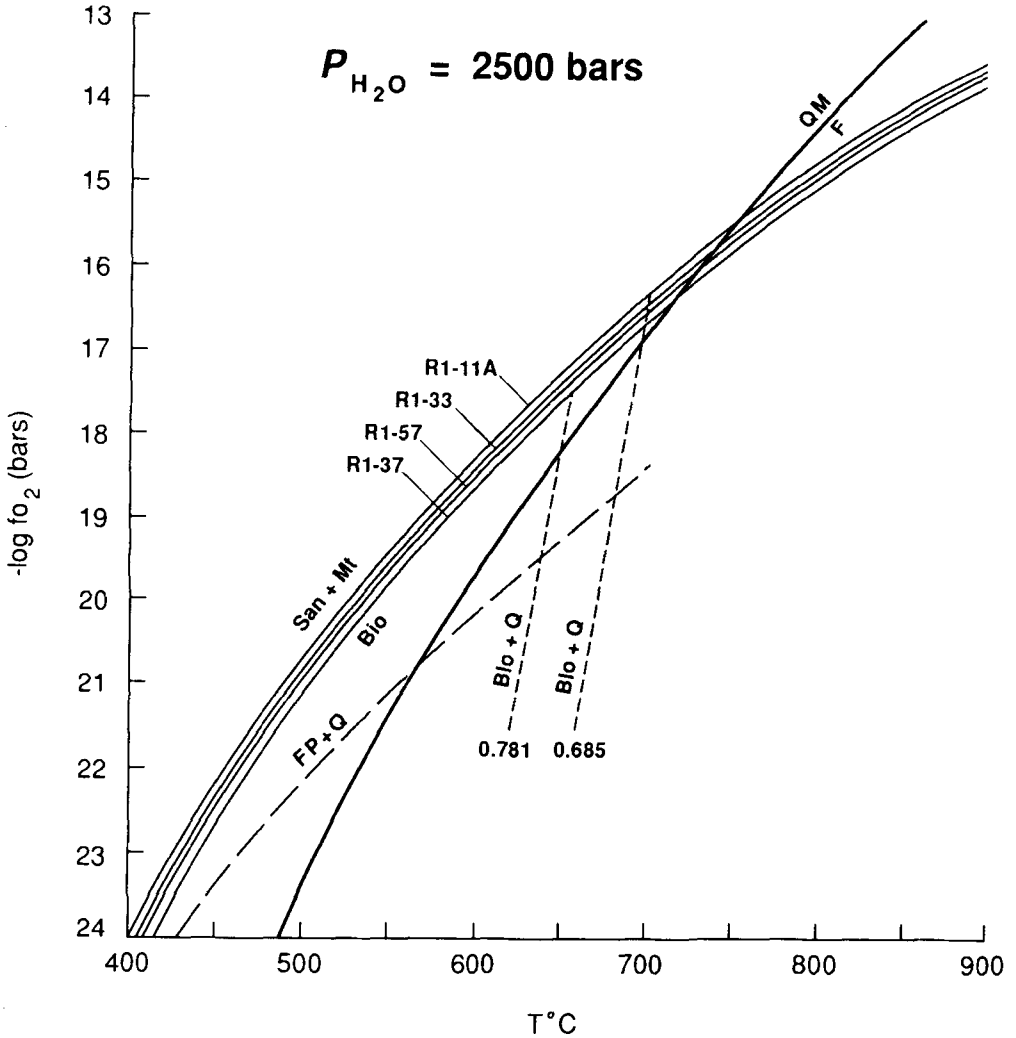


FIG. 2. T-$fO_2$ relations of biotites in the fayalite-bearing rapakivi granites, calculated from equation (3) using the data given in Table 3 and $P_{H_2O}$ = 2500 bars. QFM buffer after Hewitt (1978). Upper stability limits of biotite + quartz for the range of Fe/(Fe + Mg) ratios in the rapakivi granites are shown. Curve FP + Q shows the upper stability of synthetic ferropargasite + quartz buffered by QFM (Gilbert, 1966).

+ quartz is not stable above 553°C at $P_{H_2O}$ = 2000 bars on the QFM buffer, but this cannot be reconciled with the textural evidence which shows amphibole crystallisation to sometimes precede that of biotite. However, Gilbert (*ibid.*) has shown that more silicic and $Fe^{3+}$-rich compositions (such as ferro-edenitic hornblende, also developed in the rapakivi granites) are stable at higher temperatures, and this may help to explain the textural discrepancy. Unfortunately, precise stability ranges of Fe-rich amphiboles are not yet known and no quantitative interpretation of the data can be made.

Reaction (2) can be represented by

$$\log f_{H_2O} = \frac{-4996}{T} + 8.47 + 3 \log X_{OH}^{Bio} + 3/2 \log a_{SiO_2} - \log a_{San}^{Afsp} - 3/2 \log a_{San}^{Afsp} \quad (4)$$

(Nash, 1976; $X_{OH}^{Bio}$ term added by Parsons, 1981). $a_{SiO_2}$ was taken to be 1.0, and other terms are

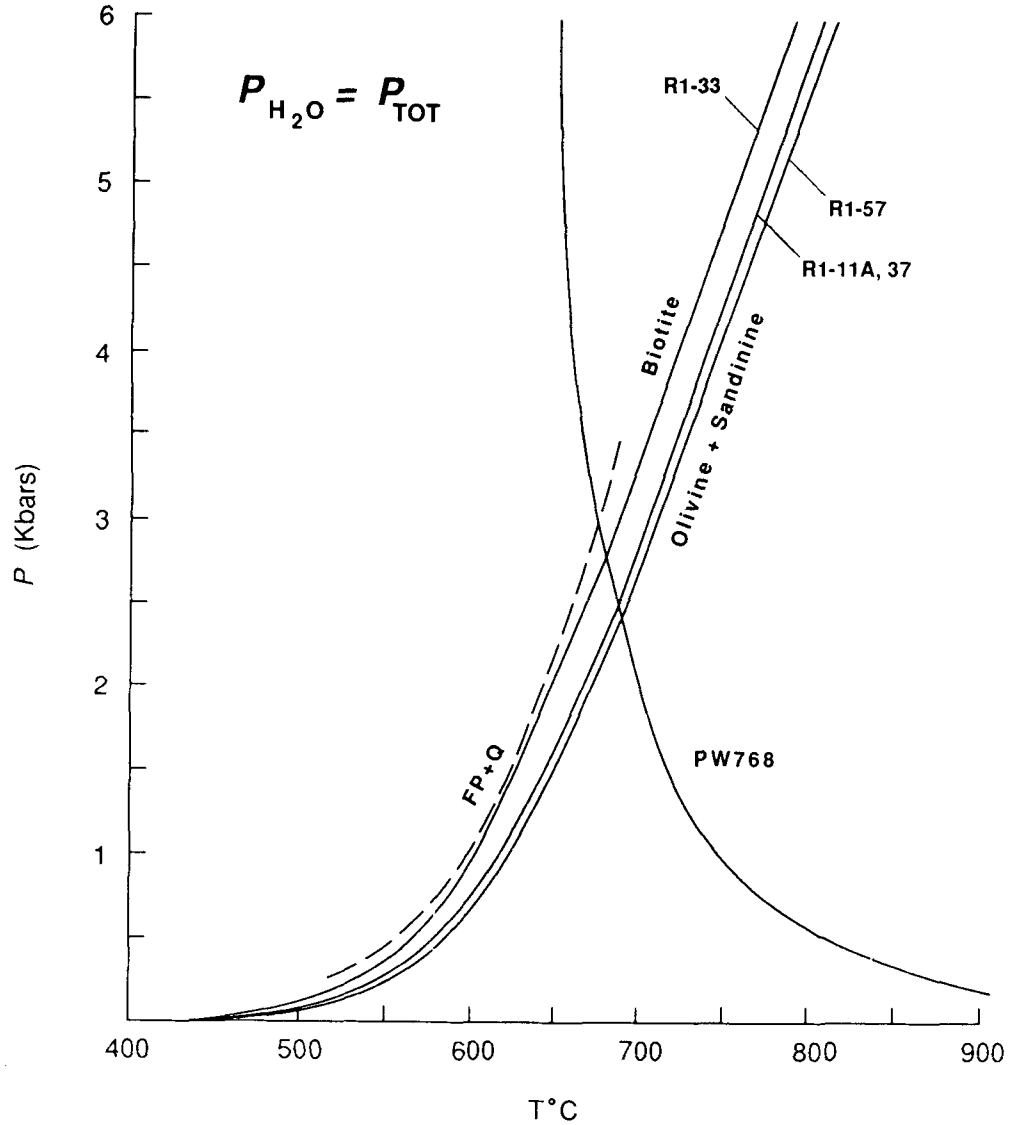


FIG. 3. Curves showing the stability limits of biotite from the fayalite-bearing rapakivi granites, calculated from equation (4) using the data given in Table 3. FP + Q shows the upper stability of synthetic ferropargasite + quartz (after Gilbert, 1966). PW768 is the water-undersaturated solidus for a natural granodiorite (Piwinskii and Wyllie, 1968).

given in Table 3; olivine was assumed to mix ideally.

Biotite stability curves calculated from equation (4) are shown in Fig. 3, and have been converted from $f_{H_2O}$ to values in $P_{H_2O}$ (assuming $P_{H_2O} = P_{TOT}$) using the data of Burnham *et al.* (1969). Assuming a minimum confining pressure of *c.* 2.5 kbar for the emplacement of the pluton (Table 1) it is clear that biotite started to crystallise at or below the solidus, at temperatures below 690–675°C; these temperatures are in good agreement with those derived from Fig. 2. Biotite continued to grow to below 450–500°C as witnessed by its preferential replacement of coarsely perthitic microcline, which will start to form at these temperatures (Brown and Parsons, 1984).

When biotite assumes a symplectic morphology it is intergrown with quartz, which suggests that the quartz-producing, olivine-consuming reaction (2) is the dominant mechanism for biotite forma-

*TABLE 4. COMPOSITION OF COEXISTING OLIVINE–ORTHOPYROXENE PAIRS*

| | Mol% Fa | Mol% Fs | $\Delta X$ | $K_{D\,ol-opx}^{Mg-Fe}$ |
|---|---|---|---|---|
| R1-4 | 0.940 | 0.824 | 0.116 | 3.395 |
| R1-11A | 0.947 | 0.838 | 0.109 | 3.440 |
| R1-11A | 0.958 | 0.819 | 0.139 | 5.001 |
| R1-11A | 0.944 | 0.824 | 0.120 | 3.597 |
| R1-33 | 0.950 | 0.830 | 0.120 | 3.354 |
| 49081(1) | 0.905 | 0.771 | 0.134 | 4.234 |
| 49297(1) | 0.902 | 0.780 | 0.122 | 3.590 |
| BS42(2) | 0.935 | 0.842 | 0.093 | 2.372 |
| BS43(2) | 0.939 | 0.829 | 0.110 | 2.982 |

$\Delta X$ = $[Fe/(Fe+Mg)]_{ol}$ – $[Fe/(Fe+Mg)]_{opx}$ (from Smith, 1971). $K_{D\,ol-opx}^{Mg-Fe}$ calculated as $(Mg/Fe)_{op}.(Fe/Mg)_{ol}$. Other analyses from (1) Frisch and Bridgwater (1976), and (2) Oyawoye and Makanjuola (1972).

tion. However, as biotite is never seen in contact with olivine, this implies localised control of the reaction through diffusion on a scale of 1–2 mm, probably through a vapour phase.

The stability of synthetic ferro-pargasite is also shown on Fig. 3 (Gilbert, 1966), and its near-coincidence with the calculated stability curves for biotite may help to explain the ambiguous textural relationships of the two minerals.

*The assemblage olivine–orthopyroxene–quartz.* The occurrence of fayalite in quartz syenites and alkaline granites is widely known, but the assemblage olivine–orthopyroxene–quartz is much less common. It is generally recorded from high-grade regional and contact metamorphic rocks (reviewed by Bohlen and Boettcher, 1981), but may also be developed in felsic plutonic rocks (e.g. Smith, 1974; Frisch and Bridgwater, 1974). Bohlen and Boettcher have presented experimentally determined stabilities for the reaction

fayalitic olivine + quartz = ferrosilite-rich orthopyroxene (+ olivine + quartz) (5)

The experimental data of Bohlen and Boettcher (1981) show that for the range of olivine compositions observed in the black rapakivi granites the upper limit of reaction (5) exceeds *c.* 6 kbar. The effects of minor components (Mn, Al, Ca) on orthopyroxene stability are negligible.

Values for the distribution coefficient $K_{Mg-Fe}^{opx-ol}$ (calculated as $[Mg/Fe]_{opx}.[Fe/Mg]_{ol}$ for olivine and orthopyroxene pairs in contact with each other are presented in Table 4. Although these are higher than the values presented by Bohlen and Boettcher for a bulk pyroxene composition of $Fs_{90}En_{10}$ (1.5 to 3.0 at 800°C), their data suggest that $K$ increases with decreasing temperature to values equivalent to those in Table 4 at granite solidus temperatures.

The value $\Delta X$ ($[Fe/Fe+Mg]_{ol}$–$Fe/[Fe+Mg]_{opx}$; Table 4, after Smith, 1971) for the Prins Christians Sund fayalite-bearing rapakivi granites is in good agreement with other natural examples of similar composition to those presented here (Oyawoye and Makanjuola, 1972; Frisch and Bridgwater, 1976), which suggests that the assemblage has reached equilibrium. Textural and chemical evidence shows this to have occurred via the consumption of olivine to form biotite (reaction 2) rather than orthopyroxene (reaction 5), since increasingly magnesian compositions are required to maintain the stability of the assemblage olivine + orthopyroxene + quartz at lower pressures (Bohlen and Boettcher, 1981).

## Conclusions

The Prins Christians Sund pluton is a post-tectonic rapakivi granite which was emplaced into early Proterozoic (*c.* 1.9 Ga) migmatitic metasediments and deformed granites around 1.73 Ga. Much of the rapakivi granite is black in hand specimen, and these rocks contain fayalite in association with Fe-rich orthopyroxene, amphibole, biotite, and rare clinopyroxene. Feldspars in the black granites are remarkably fresh and non-turbid, whereas those in a localised white facies of the granite are white and turbid. The amphibole and biotite are both subsolidus phases, and although the $T$–$f_{O_2}$ conditions for the formation of amphibole cannot be accurately determined (owing to the lack of reliable experimental data), biotite can be shown to have formed in response to a fayalite-consuming reaction at temperatures below 650–700°C and $f_{O_2}$ of $10^{-16.5}$ to $10^{-17.5}$ bars. It continued to grow under reducing conditions below the QFM buffer to temperatures below 450–500°C. Available experimental data suggest that orthopyroxene has formed from a fayalite + quartz-consuming reaction (observable in thin section) at pressures less than *c.* 6 kbar.

The association between the white granite and metasedimentary xenoliths suggests that fluids have been exchanged between the two, and that the increased fluid content in the magma resulted in the pervasive fluid interaction responsible for feldspar turbidity. Furthermore, the correlation of black, pristine feldspar with anhydrous mafic minerals, and of turbid feldspar with hydrous phases suggests that the mafic assemblages in the white granite are secondary.

**Acknowledgements**

The samples studied here were collected in July 1983 by Ian Parsons and John Teasdale (funded by NERC grant GR3/5028), and the area was revisited in August 1988 by the senior author. The work is currently funded by NERC grant GR3/6336. Aberdeen microprobe analyses have been made by George Taylor and John Still. In Edinburgh, analysis was supervised by Stuart Kearns.

## References

Allaart, J. H. (1967) Basic and intermediate igneous activity and its relationships to the evolution of the Julianehaab granite, South Greenland. *Medd. om Grønland,* 175, no. 1.

—— 1976) Ketilidian mobile belt in South Greenland. In: Escher, A. and Watt, W.S. (eds.) *Geology of Greenland.* Copenhagen: Grønlands Geologiske Undersøgelse, 120–51.

Bohlen, S. R. and Boettcher, A. L. (1981) Experimental investigations and geological applications of orthopyroxene geobarometry. *Amer. Mineral.* **66,** 951–64.

Bridgwater, D. (1963) A review of the Sydprøven granite and other 'New Granites' of South Greenland. *Medd. Dansk Geol. Foren.* **15,** 167–82.

—— Sutton, J. and Watterson, J. (1974) Crustal downfolding associated with igneous activity. *Tectonophys.* **21,** 57–77.

Brown, P. E., Tocher, F. E. and Chambers, A. D. (1982) Amphiboles from the Lilloise intrusion, East Greenland. *Mineral. Mag.* **45,** 47–54.

Brown, W. L. and Parsons, I. (1984) Exsolution and coarsening mechanisms and kinetics in an ordered cryptoperthite series. *Contrib. Mineral. Petrol.* **86,** 3–18.

Burnham, C. W., Holloway, J. R. and Davies, N. F. (1969) Thermodynamic properties of water to 1000°C and 10,000 bars. *Spec. Paper Geol. Soc. Amer.* 132.

Czamanske, G. K. and Wones, D. R. (1973) Oxidation during magmatic differentiation, Finnmarka Complex, Oslo area, Norway: Part 2, the mafic silicates. *J. Petrol.* **14,** 359–80.

Deer, W.A., Howie, R.A. and Zussmann, J. (1978) *Rock-forming minerals, 2A. Single-chain silicates* (2nd ed.) Longman, London. 688pp.

Eugster, H. P. and Wones, D. R. (1962) Stability relations of the ferruginous biotite, annite. *J. Petrol.* **3,** 82–125.

Frisch, T. and Bridgwater, D. (1976) Iron- and manganese-rich minor intrusions emplaced under late-orogenic conditions in the Proterozoic of South Greenland. *Contrib. Mineral. Petrol.* **57,** 25–48.

Furhman, M. L. and Lindsley, D. H. (1988) Ternary-feldspar modelling and thermometry. *Amer. Mineral.* **73,** 201–15.

Gilbert, M. E. (1966) Synthesis and stability relations of the hornblende ferropargasite. *Amer. J. Sci.* **264,** 698–742.

Gulson, B. L. and Krogh, T. E. (1975) Evidence of multiple intrusion, possible resetting of U-Pb ages, and new crystallisation of zircon in the post-tectonic intrusions ('Rapakivi granites') and gneisses from South Greenland. *Geochim. Cosmochim. Acta,* **39,** 65–82.

Harley, S. L. (1984) An experimental study of the partitioning of Fe and Mg between garnet and orthopyroxene. *Contrib. Mineral. Petrol.* **86,** 359–73.

Harrison, T. N., Brown, P. E., Parsons, I., Hutton, D. H. W., Dempster, T. J., and Becker, S. M. (1988) Granulite facies metamorphism, magmatism and extensional tectonics in the Ketilidian mobile belt of Southern Greenland. *Mineral. Soc. Bull.* no. 80, p. 8 (abstr.).

—— Reavy, R. J., Finch, A. A. and Brown, P. E. (in press) Coexisting mafic and felsic magmas in the early Proterozoic rapakivi granite suite of Southern Greenland *Bull. Geol. Soc. Denmark*, **38.**

Hewitt, D. A. (1978) A redetermination of the fayalite–magnetite–quartz equilibrium between 650° and 850°C. *Amer. J. Sci.* **278,** 715–24.

Leake, B. E. (1978) Nomenclature of amphiboles. *Mineral. Mag.* **42,** 533–63.

Nash, W. P. (1976) Fluorine, chlorine and OH-bearing minerals in the Skaergaard intrusion. *Amer. J. Sci.* **276,** 546–57.

Oyawoye, M. O. and Makanjuola, A. A. (1972) Bauchite: a fayalite-bearing quartz monzonite. *24th. Int. Geol. Congr.*, Section 2, 251–66.

Parsons, I. (1978) Feldspars and fluids in cooling plutons. *Mineral. Mag.* **42,** 1–17.

—— (1981) The Klokken gabbro–syenite complex, South Greenland: quantitative interpretation of mineral chemistry. *J. Petrol.* **22,** 233–60.

—— and Brown, W. L. (1984) Feldspars and the thermal history of igneous rocks. In *Feldspars and Feldspathoids* (Brown, W. L., ed.) Reidel, Berlin, 317–71.

Perkins, D. and Chipera, S. J. (1985) Garnet–orthopyroxene–plagioclase–quartz barometry: refinement and application to the English River subprovince and the Minnesota River valley. *Contrib. Mineral. Petrol.* **89,** 69–80.

Piwinskii, A. J. and Wyllie, P. J. (1968) Experimental studies of igneous rock series: a zoned pluton in the Wallowa batholith, Oregon. *J. Geol.* **76,** 205–34.

Smith, D. (1971) Stability of the assemblage iron-rich orthopyroxene–olivine–quartz. *Amer. J. Sci.* **271,** 370–82.

—— (1974) Pyroxene–olivine–quartz assemblages in rocks associated with the Nain anorthosite massif. *J. Petrol.* **15,** 58–78.

Streckeisen, A. (1976) To each plutonic rock its proper name. *Earth. Sci. Rev.* **12,** 1–33.

Windley, B. F. (1965) The composite net-veined diorite intrusives of the Julianehaab district, South Greenland. *Medd. om Grønland* **172,** no. 8.

Worden, R. H., Walker, F. D. L., Parsons, I. and Brown, W.L. (1989) Micropores and perthite coarsening. *Terra Abstracts* **1,** 290–1.

*[Manuscript received 12 May 1989; revised 26 June 1989]*